

Published in final edited form as:

Biochemistry. 2008 October 28; 47(43): 11285–11299. doi:10.1021/bi801185b.

Analysis of IgA1 *N*-glycosylation and its contribution to FcαRI binding†

Michelle M. Gomes[‡], Stephanie B. Wall[§], Kazuo Takahashi^{||}, Jan Novak^{||}, Matthew B. Renfrow^{§,*}, and Andrew B. Herr^{‡,*}

[‡] Department of Molecular Genetics, Biochemistry and Microbiology, University of Cincinnati College of Medicine, Cincinnati, OH 45267-0524

[§] Biomedical FT-ICR Mass Spectrometry Laboratory, Department of Biochemistry and Molecular Genetics, University of Alabama at Birmingham, Birmingham, AL 35294

^{||} Department of Microbiology, University of Alabama at Birmingham, Birmingham, AL 35294

Abstract

The IgA isotype of human antibodies triggers inflammatory responses via the IgA-specific receptor FcαRI (CD89). Structural studies have suggested that IgA1 *N*-glycans could modulate the interaction with FcαRI. We have carried out detailed biophysical analyses of three IgA1 samples purified from human serum and recombinant IgA1-Fc and compared their binding to FcαRI. Analytical ultracentrifugation revealed wide variation in the distribution of polymeric species between IgA1 samples, and Fourier transform ion cyclotron resonance mass spectrometry showed overlapping but distinct populations of *N*-glycan species between IgA1 samples. Kinetic and equilibrium data from surface plasmon resonance experiments revealed that variation in the IgA1 C_H2 *N*-glycans had no effect on the kinetics or affinity constants for binding to FcαRI. Indeed, complete enzymatic removal of the IgA1 *N*-glycans yielded superimposable binding curves. These findings have implications for renal diseases such as IgA nephropathy.

Keywords

FcαRI; IgA1; IgA nephropathy; *N*-glycosylation; mass spectrometry; analytical ultracentrifugation; surface plasmon resonance

IgA antibodies play an important role in protecting against environmental pathogens and antigens encountered at mucosal sites (1). IgA is the second most prevalent antibody in the serum after IgG and is divided into two subclasses, IgA1 and IgA2. There are several distinct forms of IgA; monomeric, dimeric or higher polymeric forms are found in serum, and secretory IgA is found in mucosal secretions. Monomeric IgA consists of two heavy chains and two light chains, κ or λ. Each IgA heavy chain has an extended C-terminal tailpiece, which can form an intermolecular disulfide bond with joining (J) chain leading to the formation of dimeric or polymeric IgA. In serum, approximately 95% of IgA is monomeric and 5% is polymeric (1, 2). The IgA1 subclass contains an *O*-glycosylated hinge region connecting the Fc and Fab regions as well as two conserved *N*-glycosylation sites per heavy chain: one at residue N263

†This work was supported by NIH grants DK071802, DK078244, DK080301, DK061525, DE013694, DK047322, and DK064400 and funds from the State of Ohio Eminent Scholar Program.

*To whom correspondence should be addressed. M.B.R.: E-mail: Renfrow@UAB.edu; Phone: 205-996-4681. A.B.H.: E-mail: Andrew.Herr@UC.edu; Phone: 513-558-5312; Fax: 513-558-1190.

in the C_H2 domain and the other at N459 in the tailpiece. IgA2 has a truncated hinge region lacking *O*-glycans and an additional two or three conserved *N*-glycans (3,4).

Inflammatory responses triggered by IgA1 or IgA2 are primarily mediated by the IgA-specific Fc receptor, FcαRI. FcαRI is a type I transmembrane glycoprotein expressed on cells of the myeloid lineage including eosinophils, neutrophils, monocytes and macrophages (5,6). It consists of two extracellular immunoglobulin-like domains, a transmembrane domain with a positively charged arginine residue that associates with the Fcγ-chain signaling co-receptor, and a short cytoplasmic tail (1). Activation of FcαRI on myeloid cells by IgA immune complexes triggers inflammatory immune responses such as phagocytosis, respiratory burst, antibody-dependent cellular cytotoxicity (ADCC) and cytokine release (1). In addition, cross-linking of cell surface FcαRI by IgA immune complexes causes the shedding of the extracellular domain of FcαRI into circulation (7). This soluble FcαRI still retains its capacity to bind IgA1 and can associate with polymeric IgA1, creating soluble IgA-FcαRI complexes in circulation (8).

Recently, we solved the crystal structure of soluble FcαRI bound to an IgA1-Fc core fragment (called Fcα) at 3.1 Å (9). The N-terminal domain of FcαRI (D1) binds IgA in the C_H2/C_H3 junction of Fcα, as predicted by mutational work (9,10). Two FcαRI molecules bind a single IgA homodimer, which is consistent with prior analytical ultracentrifugation (AUC) and surface plasmon resonance (SPR) studies (11). Although Fcα generally resembles IgG-Fc (Fcγ) and IgE-Fc (Fcε), the location of the C_H2 domain *N*-glycans differs dramatically. The Fcα *N*-glycans are located on the external surface of the C_H2 domains (Figure 1A), unlike Fcγ and Fcε *N*-glycans, which are found between the upper Fc domains (9,12,13). Furthermore, the C_H2 *N*-glycans on Fcα are solvent-accessible and approach within 8 Å of FcαRI. However, the electron density for the Fcα *N*-glycans in the crystal structure was weak and only one branch of the putative biantennary oligosaccharide could be resolved. Thus, the C_H2 *N*-glycans of IgA1 may directly contact FcαRI and play a role in the FcαRI-IgA1 interaction. In contrast to the IgA1 *N*-glycans, the *O*-glycosylated hinge region is located 20–30 Å from FcαRI (based on superposition of the Fcα:FcαRI crystal structure (9) and the solution structure of IgA1 determined by small-angle X-ray and neutron scattering (14), and thus would not be expected to interact with FcαRI at all (Figure 1B).

The physiological role of IgA1 glycosylation is unclear, outside of IgA clearance by hepatocytes via the asialoglycoprotein receptor (15) and glycan-dependent immune exclusion by secretory IgA (2,16). However, abnormalities in glycosylation have been implicated in several diseases such as Sjögren's syndrome (17), Henoch-Schönlein purpura (18–20) and IgA nephropathy (IgAN) (20,21). IgAN is the best-understood example of a disease whose pathogenesis has been linked to aberrant IgA1 glycosylation. This disease is characterized by the deposition of IgA1-containing immune complexes in the glomerular mesangium, resulting in mesangial cell proliferation, matrix overproduction, and infiltration of inflammatory immune cells (22,23). The mechanisms leading to IgA1 deposition in the kidney are still unclear; however, altered glycosylation and polymerization states of IgA1 and immune complex formation have been reported in a large number of IgAN patients. Aberrancies in IgA1 glycans in IgAN include galactose deficiency of *O*-linked glycans (20,24–26), sometimes reported to be accompanied by either oversialylation (27) or undersialylation (28,29). One of these studies (28) also indicated that *N*-linked glycans of IgA may be affected. These alterations in IgA1 may affect its interaction with receptors; indeed, IgA1 from IgAN patients has been reported to show either increased (30) or decreased (31) binding to FcαRI, and increased binding to transferrin receptor (32). Altered IgA1 affinity for cellular receptors could have important implications for immune complex formation, mesangial deposition of IgA1, and pathogenesis of IgAN. For example, soluble FcαRI complexed with IgA has been implicated in pathogenesis in a mouse model of IgAN (33), and transferrin receptor has been identified

as a mesangial cell receptor capable of binding IgA1 from IgAN patients (34). However, there is some level of controversy about the role of these receptors in IgAN. Circulating Fc α RI:IgA1 complexes are present in healthy subjects as well as in patients with IgAN, and no correlation between levels of circulating IgA1-Fc α RI complexes and IgAN prognosis was found (35). Furthermore, mouse IgA failed to bind Fc α RI under conditions favoring binding of human IgA (36), raising questions about the conclusions of the human Fc α RI transgenic mouse model of IgAN.

Given the aberrant glycosylation of IgA1 in IgAN, the suggested role of soluble Fc α RI in the disease, and the possible interaction between IgA1 *N*-glycans and Fc α RI suggested by the crystal structure, we set out to characterize the contribution that IgA1 *N*-glycans make to the IgA1-Fc α RI interaction. We have analyzed the polymeric state and *N*-glycosylation profile of different human myeloma IgA1 proteins using analytical ultracentrifugation (AUC) and Fourier transform ion cyclotron resonance mass spectrometry (FT-ICR MS), respectively. Furthermore, we have compared the Fc α RI binding affinities of a recombinant IgA1-Fc fragment and the three purified human IgA1 samples through extensive kinetic and equilibrium binding analyses by surface plasmon resonance (SPR). Finally, we have compared the Fc α RI binding affinity of a human IgA1 sample before and after enzymatic removal of the *N*-glycans to assess their contribution to the interaction with Fc α RI.

Experimental Procedures

IgA1 purification

Myeloma patient-derived IgA1 κ and λ proteins were obtained from Biodesign International (Cincinnati, OH). IgA1 (Mce), a naturally undergalactosylated myeloma IgA1 protein that resembles IgA1 from IgAN patients, was isolated as described (21). Each protein was purified by size exclusion chromatography using a Hi Load 16/60 Superdex 200 column (Amersham Biosciences) into monomeric, dimeric/trimeric and high-molecular weight fractions. Size exclusion-purified monomeric IgA1 (mIgA1) fractions were used for binding experiments and are referred to as mIgA1 κ , mIgA1 λ , and mIgA1_{Mce}.

Fc α vector, transfection, expression and purification

The core IgA1-Fc fragment (called Fc α) lacking hinge and tailpiece regions has been described previously (11). This construct was sub-cloned into the pcDNA3 vector using EcoRI and HindIII restriction sites. COS-7 cells were grown in Dulbecco's modified Eagle's medium (DMEM) and supplemented with 10% fetal bovine serum (FBS) and 1% penicillin-streptomycin. The COS-7 cells were transfected with 5 μ g of Fc α vector using Lipofectamine 2000 reagent (Invitrogen) according to the manufacturer's instructions. 72 h after transfection, stable cells were selected with 500 μ g/ml G418. Western blots using anti-IgA1 (Southern Biotech, Birmingham, AL) showed expression of Fc α . Culture medium was harvested from the stably transfected cells and dialyzed against 20 mM Tris, 150 mM NaCl, pH 7.4 (TBS). Fc α was purified by two sequential Ni-affinity chromatography steps, followed by size exclusion chromatography using a Superdex 200 column (Amersham Biosciences). Purity of the protein was determined to be >95% by SDS-PAGE. Protein concentrations were determined using extinction coefficients of 64,940 M⁻¹ cm⁻¹ for Fc α (11) and 208,280 M⁻¹ cm⁻¹ for mIgA1 (14).

Fc α RI purification

Soluble recombinant Fc α RI ectodomain was expressed in baculovirus-infected insect cells by the Caltech Protein Expression Center and purified by Ni-affinity chromatography followed by size exclusion chromatography (11). The resulting Fc α RI was monomeric based on size exclusion chromatography and AUC analyses and was estimated to be > 95% pure by SDS-

PAGE. Fc α RI concentration was calculated using an extinction coefficient of 33,140 M⁻¹ cm⁻¹.

Enzymatic Deglycosylation of IgA1 N-glycans

Forty μ g of serum-derived mIgA1 κ was incubated overnight at 37° C in 100 mM sodium phosphate buffer (pH 7.5) with 0.08 U of PNGase F (*N*-glycanase; Glyko, San Leandro, CA) in the presence or absence of 0.3 U α -L-fucosidase (Sigma). One-hundred ng of mIgA1 κ before and after enzymatic treatment was separated by SDS-PAGE under reducing conditions and stained with Coomassie blue to verify the expected decrease of the apparent molecular mass of the heavy chain after deglycosylation.

Mass spectrometry

For analysis of IgA1 *N*-glycosylation by reversed phased C18 liquid chromatography (LC) FT-ICR MS, IgA1 glycopeptides were analyzed as tryptic fragments as described (37). The glycopeptide amino acid sequence was confirmed by use of activated ion-electron capture dissociation (AI-ECD) FT-ICR tandem mass spectrometry (MS/MS) as previously described (37), with the exception that the precursor ion populations were photon-irradiated for 100 ms at 8% (1.6 W) laser power. Individual *N*-glycans were identified from the known sequence of the isolated *N*-glycopeptide and monoisotopic mass assignment of glycopeptides by use of the GlycoMod tool (<http://www.expasy.org>). Methods for analysis of PNGase F-released IgA1 *N*-glycans by use of FT-ICR MS and LTQ tandem mass spectrometry (MS/MS) are described in supplemental material.

Carbohydrate analyses

The monosaccharide composition of glycans of mIgA1 κ , mIgA1 λ , and mIgA1_{Mce} proteins were determined as trifluoroacetates of methylglycosides by gas-liquid chromatography (38, 39). All monosaccharides were quantified relative to the total protein and their ratios were expressed relative to mannose.

Analytical Ultracentrifugation

To yield the size distribution of all components of myeloma patient-derived IgA1 (κ , λ and Mce), proteins were analyzed by sedimentation velocity experiments in a Beckman XL-I ProteomeLab analytical ultracentrifuge as described (11). 400 μ l of IgA1 κ , λ and Mce were spun at 36,000 rpm at 20° C and scanned at 230 nm. Data were fitted using the *c*(*s*) and *c*(*M*) analysis routines in the program SEDFIT, which calculates the differential distribution of sedimentation coefficients or apparent molecular masses after accounting for sample diffusion (40). Each initial IgA1 sample, as well as each monomeric, dimeric and polymeric sub-fraction obtained by size-exclusion chromatography, was subjected to sedimentation velocity analysis to determine the sedimentation coefficients of the sedimenting species.

Biosensor Analyses

Surface plasmon resonance (SPR) biosensor assays were carried out on a Biacore 3000 instrument. For all experiments, 10 μ g/ml Fc α , mIgA1 κ , mIgA1 λ , or mIgA1_{Mce} were diluted in sodium acetate buffer (pH 4.5) and immobilized on CM-5 chips (~300 RU for Fc α and ~600 RU for mIgA1) using random amine chemistry. Previous studies showed that binding parameters derived from oriented and random amine coupling were similar (11). The first flow cell was mock-coupled and its response was subtracted from all other flow cells, followed by subtraction of a buffer blank injection. Soluble Fc α RI ectodomain was injected at 25 °C at concentrations ranging from 1 nM to 2.2 μ M with a flow rate of 30 μ l/minute.

The association and dissociation phases of the kinetic sensogram data were fitted using the bivalent ligand model in the program ClampXP version 3.50 (Tom Morton and David Myszk, University of Utah, 2002), which describes sequential binding of two receptor molecules to a homodimeric ligand (*i.e.*, Fc α or mIgA1). Each binding site is distinguishable (*i.e.*, not constrained to have identical affinity) and is defined as having equal occupancy. Initial binding experiments were carried out with the standard buffer TBS-P (TBS with 0.005% P20 detergent). Data from SPR chips coupled at three different densities (27 binding curves) were fitted globally using the program ClampXP (41) to yield binding parameters for mIgA1 κ . Control experiments at different flow rates indicated that the binding was not mass transport limited (11). Salt dependence experiments used 50 mM Tris-HCl (pH 7.4) with 10 mM, 30 mM, 100 mM, 300 mM, or 1 M NaCl and 0.005% P-20. For pH dependence experiments a triple buffer was utilized containing 25 mM sodium acetate, 25 mM MES, and 25 mM bis-Tris propane, adjusted to several pH values ranging from 5.5 to 9.5, with 150 mM NaCl and 0.005% P20. The apparent kinetic rate constants reported by ClampXP were corrected by appropriate statistical factors (*i.e.*, the corrected value $k_{1on} = 0.5 * k_{1on, app}$ as derived from ClampXP; corrected $k_{2off} = 0.5 * k_{2off, app}$), as described (11).

Although the kinetic fits do not perfectly overlay the observed data, they are quite reasonable given the fast kinetics and the complexity of the system. We have globally fitted two sets each of association and dissociation rate constants per dataset, and in appropriate cases we globally fitted multiple datasets from different surfaces. If a single-site model was used instead to fit the same data, the residuals were much worse unless we allowed numerous bulk refractive index (RI) shifts, which was not warranted based on the experimental design. Furthermore, adding in the bulk RI shifts increased the % error of the rate constants by 2-3-fold or more, and in some cases prevented the determination of a single best-fit set of parameters.

For equilibrium analyses, the equilibrium response (R_{eq}) at each injected analyte concentration was averaged over 60 seconds using the program Scrubber version 2 (BioLogic Software, 2005), and the binding isotherms were fitted to equations describing a two-site model in the program Scientist (Micromath Scientific Software, Salt Lake City, Utah), as described (11). Briefly, this model assumes two distinguishable sites with equal occupancy and yields the microscopic affinities for each binding event. Data from three independent experiments were fit globally to yield equilibrium-binding affinities for mIgA1 κ . The binding isotherms were shallow (*i.e.*, broader than a single-site isotherm), as expected for two non-identical sites without positive cooperativity. To illustrate this, a 1:1 binding isotherm should go from 10% occupancy to 90% occupancy over an 81-fold range in ligand concentration (as dictated by the binding equation: % bound = $Kx / (1+Kx)$). In the binding isotherm shown (Figure 3B), the curve increases from 10% to 90% bound over a ~200-fold range of Fc α RI concentration (9 nM to 2 μ M).

Thermodynamic analyses

Determination of salt and pH dependence of binding was carried out at 25 °C as described (11). The electrostatic contribution to the overall free energy of binding was determined by comparing the ΔG at 10 mM NaCl to that at 1 M NaCl, conditions under which electrostatic interactions are abolished (42). For pH studies, log K versus pH was plotted. The slope of this plot (between pH 5.5 and pH 7.5) yields $-\Delta H^+$, where ΔH^+ is the net number of protons bound or released when Fc α RI binds to Fc α . The pH dependence of binding can be described as linked equilibria by the following equation (11):

$$K_{b,obs} = K_b \frac{1 + 10^{(pK_a2)_b - pH} + 10^{pH - (pK_a1)_b}}{1 + 10^{(pK_a2)_f - pH} + 10^{pH - (pK_a1)_f}}$$

where $K_{b, obs}$ is the observed binding constant as a function of pH. Fitting our binding data to this equation, with two independent ionizable residues at each receptor binding site on Fc α or mIgA1 yields the following parameters; K_b , binding constant of Fc α RI to Fc α or mIgA1 in the unprotonated state; $(pK_a1)_f$ and $(pK_a2)_f$, the pK $_a$'s of the two ionizable residues in the free state; and $(pK_a1)_b$ and $(pK_a2)_b$ the pK $_a$'s of the two ionizable residues in the bound state.

Results

Sedimentation velocity analysis of myeloma patient-derived IgA1 κ , λ and Mce

To determine the oligomeric species present in each serum-derived IgA1 sample, IgA1 κ , IgA1 λ and IgA1 $_{Mce}$ were subjected to sedimentation velocity experiments in an analytical ultracentrifuge. The data were analyzed using the c(s) size distribution analysis method in the program SEDFIT (40). Distinct peaks corresponding to monomeric, dimeric, and trimeric IgA1, as well as high-molecular-weight forms (presumably aggregates) could be resolved in all the three samples, although the relative levels varied considerably (Figure 2). The apparent sedimentation coefficients of the species present in each IgA1 sample are listed in Supplementary Table S1. Perhaps due to its undergalactosylated state, the IgA1 $_{Mce}$ distribution was skewed towards dimeric and trimeric species and also showed high levels of very large-molecular-weight species. For binding analyses, each IgA1 sample was further purified by size exclusion chromatography and the monomeric fraction was used.

SPR analysis of Fc α RI binding to Fc α and mIgA1 κ

Kinetic and equilibrium SPR experiments were carried out in order to compare the binding of soluble Fc α RI to either recombinant Fc α or serum-purified intact mIgA1 κ (Figure 3A). For kinetic analyses, a bivalent ligand model was used to derive the rate constants and a statistical correction was applied, as described (11) (Table 1). The K_{DS} for Fc α binding to Fc α RI are 60.4 ± 0.3 nM and 121 ± 1 nM, while those for mIgA1 κ binding to Fc α RI are 74.9 ± 0.4 nM and 244 ± 4 nM for the first and second binding events, respectively. For equilibrium binding analyses, the steady-state response at each injected Fc α RI concentration was measured, and the resulting binding isotherms were fitted to a two-site binding model (Figure 3B and Table 2). Fc α binds Fc α RI with K_{DS} of 36.1 ± 1.6 nM and 204 ± 15 nM, whereas serum-purified intact mIgA1 κ binds Fc α RI with K_{DS} of 40.2 ± 1.9 nM and 452 ± 58 nM. Both kinetic and equilibrium analyses indicate that mild negative cooperativity exists between the two binding sites, as seen previously in SPR analyses of Fc α RI binding to Fc α (11). Based on both the kinetic and equilibrium analyses, Fc α and mIgA1 κ bind Fc α RI with similar, although not identical affinities. The differences between the affinities may be due to the presence of the tailpiece in mIgA1 κ , which is lacking in the Fc α fragment used here. Alternatively, differences between the *N*-glycans between recombinant Fc α (expressed in COS-7 cells) and human mIgA1 κ could play a role.

Effect of electrostatics on Fc α :Fc α RI and mIgA1 κ :Fc α RI interactions

To look for subtle differences between Fc α and mIgA1 κ binding to Fc α RI, the electrostatic contribution to the binding interaction was examined. The solution scattering study of IgA1 by Boehm et al. suggested that the tailpiece of IgA1 is likely to fold back close to the receptor binding site (14). Therefore, as the tailpiece contains a histidine, two acidic residues, and potential negatively-charged sialylated *N*-glycans, the presence of the tailpiece within the IgA1-Fc α RI interface would be expected to confer a significant electrostatic component of binding. To determine the electrostatic contribution to the binding free energy, we carried out kinetics-based biosensor binding experiments with different concentrations of NaCl in the running buffer ranging from 10 mM NaCl to 1 M NaCl; 1 M NaCl is widely accepted to effectively screen charge-charge interactions (42). The logarithms of the equilibrium association constants for Fc α or mIgA1 κ binding to Fc α RI were plotted as a function of log

[NaCl]. The slope (SK_{obs}) of each of these plots gives the net number of Na^+ and Cl^- ions taken up or released upon binding of $\text{Fc}\alpha\text{RI}$ to $\text{Fc}\alpha$ or $\text{mIgA1}\kappa$ (42) (Figure 3C). The salt dependence of $\text{mIgA1}\kappa:\text{Fc}\alpha\text{RI}$ interaction yielded slopes of -0.47 and -0.53 for the sequential binding events while the $\text{Fc}\alpha:\text{Fc}\alpha\text{RI}$ interaction had slopes of -0.32 and -0.36 , respectively. These shallow slopes for both $\text{mIgA1}\kappa$ and $\text{Fc}\alpha$ binding to $\text{Fc}\alpha\text{RI}$ suggest a minor role for counterion release upon complex formation (Table 3). The overall electrostatic contribution to the free energy of binding was calculated by comparing the Gibbs free energy (ΔG) for binding of $\text{Fc}\alpha\text{RI}$ to $\text{Fc}\alpha$ or $\text{mIgA1}\kappa$ at 10mM and 1 M NaCl . Less than 15% of the ΔG of binding for each interaction was contributed by electrostatics, and no significant difference was seen between the $\text{Fc}\alpha:\text{Fc}\alpha\text{RI}$ and $\text{mIgA1}\kappa:\text{Fc}\alpha\text{RI}$ interactions.

Effect of pH on $\text{Fc}\alpha:\text{Fc}\alpha\text{RI}$ and $\text{mIgA1}\kappa:\text{Fc}\alpha\text{RI}$ interactions

To compare the number of ionizable residues in the $\text{Fc}\alpha:\text{Fc}\alpha\text{RI}$ and $\text{mIgA1}\kappa:\text{Fc}\alpha\text{RI}$ binding interfaces, pH studies were carried out as described (11). Kinetics-based biosensor experiments were performed over a pH range from 5.5 to 9.5. The logarithm of the association constants (K_A) were plotted as a function of pH, yielding sigmoidal plots (Figure 3D). The affinities of both $\text{mIgA1}\kappa$ and $\text{Fc}\alpha$ for $\text{Fc}\alpha\text{RI}$ decreased as the pH was lowered from 7.0 to 5.5 (at pH 5.5, $K_{D1} = 803\text{ nM}$, $K_{D2} = 3.43\text{ }\mu\text{M}$ for $\text{Fc}\alpha$; and $K_{D1} = 837\text{ nM}$, $K_{D2} = 2.53\text{ }\mu\text{M}$ for $\text{mIgA1}\kappa$ binding to $\text{Fc}\alpha\text{RI}$). The negative slope of these plots (ΔH^+) describes the net number of protons (H^+ ions) released or taken up upon binding of $\text{Fc}\alpha\text{RI}$ to $\text{Fc}\alpha$ or $\text{mIgA1}\kappa$. The values of ΔH^+ for $\text{Fc}\alpha\text{RI}$ binding to $\text{Fc}\alpha$ and $\text{mIgA1}\kappa$ are approximately -1 for both sequential binding events, suggesting the presence of a single ionizable residue below pH 7.0 in the binding interface as previously reported (11), indicating the tailpiece does not contribute additional ionizable residues to the interface. The data were also fitted to a model describing linked protonation and binding equilibria (43) as described (11). Given the slight decrease in affinity at high pH as well as the large decrease at low pH, we used a model with two protonation events. This model yields K_{b1} and K_{b2} , the dissociation constants for the first and second binding events between $\text{Fc}\alpha\text{RI}$ and $\text{Fc}\alpha$ or $\text{mIgA1}\kappa$ in the unprotonated state. The low-pH transition is described by $(pK_a1)_f$ and $(pK_a1)_b$, the pK_a values for the ionizable residue when $\text{Fc}\alpha\text{RI}$ and $\text{Fc}\alpha$ or $\text{mIgA1}\kappa$ are free or bound, respectively. Likewise, $(pK_a2)_f$ and $(pK_a2)_b$ describe the high-pH transition in the free and bound states, respectively. The fitted values for $\text{Fc}\alpha\text{RI}$ binding to $\text{Fc}\alpha$ and $\text{Fc}\alpha\text{RI}$ binding to $\text{mIgA1}\kappa$ are very similar (Table 4). The pH dependence of binding for both complexes are consistent with the presence of an ionizable residue in each interface with a free pK_a value of 6.3–6.5 that becomes buried in the complex; this agrees with the $\text{Fc}\alpha:\text{Fc}\alpha\text{RI}$ crystal structure that revealed the burial of His85 of $\text{Fc}\alpha\text{RI}$ in a primarily hydrophobic pocket on $\text{Fc}\alpha$ (9). The high-pH protonation event is likely due to the $\text{Fc}\alpha\text{RI}$ N-terminus and has very little effect on binding affinity of $\text{Fc}\alpha\text{RI}$ for $\text{Fc}\alpha$ or $\text{mIgA1}\kappa$.

FT-ICR mass spectrometry analysis of N-glycan populations of $\text{mIgA1}\kappa$ and $\text{mIgA1}\lambda$

In order to analyze the importance of IgA1 *N*-glycosylation in the interaction with $\text{Fc}\alpha\text{RI}$, we first carried out a detailed analysis of the populations of *N*-glycans present on mIgA1 samples by monosaccharide compositional analysis and LC FT-ICR MS. Gas-liquid chromatographic analysis identified fucose, mannose, galactose, *N*-acetylgalactosamine, *N*-acetylglucosamine, and sialic acid in the preparations of mIgA1 , indicating the presence of both *N*-linked and *O*-linked glycans. $\text{mIgA1}_{\text{Mce}}$ had more galactose and *N*-acetylgalactosamine and less sialic acid compared to $\text{mIgA1}\kappa$. Relative proportion of mannose to other monosaccharides suggested absence of high-mannose glycans. *N*-glycans of $\text{mIgA1}\kappa$ and λ were then analyzed as glycopeptide tryptic fragments. IgA1 *N*-glycopeptides were identified by accurate mass and simultaneous data-dependent MS/MS of candidate glycopeptides, as previously described for IgA1 *O*-glycopeptides (37). This approach allowed confirmation of specific ion species as *N*-glycosylated peptides and provided *N*-glycan structural information as well (Figure 4). The dominant series of fragments originated from the terminal end of the *N*-glycan and allowed a

stepwise assignment of the *N*-glycan structure. While the LTQ MS/MS spectra do not distinguish between galactose and mannose residues, our monosaccharide compositional analysis detected the presence of both sugars, in ratios consistent with the presence of the well-established GlcNAc₂Man₃ core of predominantly complex glycans. IgA1 *N*-glycans were also removed by PNGase F treatment and analyzed by direct infusion FT-ICR MS, LTQ MS/MS and infra-red multiphoton dissociation (IRMPD) FT-ICR MS/MS (see supplemental Figures S1 and S2). The same *N*-glycan covalently linked to the IgA1 tryptic fragment in Figure 4 was analyzed by IRMPD MS/MS as a released *N*-glycan (Figure 4B). A similar fragment ion series indicating the same *N*-glycan structure as Figure 4A was observed. Additionally, fragments from the reducing end of the chain were observed.

In the course of cataloguing the individual IgA1 *N*-glycopeptide species, several of them could not be identified based on the theoretical mass of expected IgA1 tryptic fragments with attached *N*-glycans. AI-ECD fragmentation of these candidate glycopeptides was performed to confirm the amino acid sequence (Figure 5). All together, the combination of *N*-glycopeptide, *N*-glycan, and base peptide analyses provided high confidence in all of the assigned IgA1 *N*-glycans, as summarized in Table 5. Analysis of the glycopeptides revealed that mIgA1κ and mIgA1λ had overlapping but distinct patterns of *N*-glycosylation, including biantennary, triantennary, and tetraantennary complex carbohydrates (Figure 5 and Table 5).

Analysis of tryptic glycopeptides revealed a wide range of N459 (tailpiece) *N*-glycoforms that were similar between mIgA1κ and mIgA1λ, although only mIgA1λ exhibited tetraantennary *N*-glycans. In contrast, only a single highly abundant *N*-glycopeptide was observed for the C_H2 (N263) site among the tryptic glycopeptides. The amino acid sequence surrounding this site has a predicted negative charge. As a result, there could be several N263 glycopeptide species that would go undetected in positive ion MS. Analysis of the released *N*-glycans did reveal several additional *N*-glycans not observed as glycopeptides for both IgA1 proteins (Table 5). These glycans include three non-fucosylated biantennary *N*-glycans and one fucosylated triantennary *N*-glycan from mIgA1κ that were not observed for the tailpiece *N*-glycans. For mIgA1λ, one biantennary and three triantennary non-fucosylated *N*-glycans were identified that were not observed among its tailpiece glycans. Of significant note is that only one *N*-glycan with two sialic acid residues was observed in the released glycans, in contrast to the seven *N*-glycans observed as *N*-glycopeptides with two and three sialic acid residues. The presence of the peptide attached to the glycan provides more sites to be protonated in the ionization process. For the *N*-glycans indirectly assigned to the C_H2 site, this would indicate that there are more non-fucosylated *N*-glycans with two and three sialic acid residues present, but we were not able to detect them in positive ion MS. In general, more than 90% of the tailpiece glycans of both mIgA1κ and mIgA1λ were fucosylated, consistent with previous data (44), whereas only one fucosylated *N*-glycan was observed among all the C_H2 glycans,

In addition to the qualitative assessment of the *N*-glycan chains at each site, the MS analysis can provide relative quantitative information on the population of *N*-glycoforms present within a single sample and compared to each other. Figure 6 is a comparison of two independent LC-MS analyses of mIgA1κ and mIgA1λ. Biantennary *N*-glycopeptides were the most abundant *N*-glycans observed on mIgA1κ at the tailpiece site. For mIgA1λ, the triantennary *N*-glycopeptides dominate the population of IgA1 *N*-glycans at the tailpiece. Figures 6A and B demonstrate these observations in the FT-ICR MS spectra at two different points in the aligned chromatograms. In Figure 6A, the mIgA1κ spectrum shows the *N*-glycopeptide L112-M123 with *N*-glycans that differ only by a single GlcNAc residue (i.e., biantennary vs. triantennary). For mIgA1κ, only the biantennary *N*-glycopeptide is present with no triantennary glycoform observed. For mIgA1λ, both *N*-glycoforms are observed but the triantennary form dominates. In Figure 6B, the same trend holds for the same IgA1 tryptic glycopeptide with an additional sialic acid residue that elutes later in the LC-MS analysis. This shift towards a higher branched

population in mIgA1 λ is further supported by detection of tetraantennary forms. The same trend of a higher branched population in mIgA1 λ compared to mIgA1 κ is observed in the released *N*-glycans (data not shown). Thus, although the populations of IgA1 *N*-glycoforms at the tailpiece are qualitatively similar, there are distinct differences in their relative abundances within each sample. This is also true for the *N*-glycans indirectly assigned to the C_H2 site.

SPR analyses of Fc α RI binding to three serum-derived mIgA1 species (κ , λ and Mce)

Given the heterogeneity of *N*-glycosylation at the C_H2 site, SPR kinetic and equilibrium experiments were performed to compare the binding affinities of Fc α RI for mIgA1 κ , mIgA1 λ , and mIgA1_{Mce}. Each of these IgA1 samples are of the same isotype and thus will have the same amino acid sequence in their Fc region, so the only relevant differences between samples would be due to *N*-glycan variability. Our data from kinetic experiments showed very similar association and dissociation constants for Fc α RI binding to all the three IgA1 monomer samples (Table 1). Furthermore, our equilibrium analyses showed very similar affinities for Fc α RI binding to IgA1 κ , λ and Mce monomer; indeed, the equilibrium binding isotherms almost perfectly overlaid (Figure 3B; Table 2). Analysis of the salt dependence of binding showed very similar slopes for each IgA1 sample (Table 3), indicating similar electrostatic interactions.

Enzymatic deglycosylation of IgA1 *N*-glycans does not affect its interaction with Fc α RI

To establish more conclusively whether the *N*-glycans of IgA1 modulate the interaction with Fc α RI, we enzymatically removed the IgA1 *N*-glycans (Figure 7A). Gas chromatographic analysis of the final deglycosylated sample confirmed that about 85-87% of the *N*-glycans were removed (data not shown). Kinetic SPR analyses revealed similar on- and off-rates for the binding of Fc α RI to untreated or deglycosylated IgA1, and the calculated dissociation constants were nearly identical, indicating that loss of the *N*-glycans had essentially no effect on the binding affinity (Table 1). Furthermore, equilibrium SPR binding analyses of the native and deglycosylated samples gave superimposable binding curves (Figure 7C; Table 2). Finally, the salt dependence of the native and deglycosylated IgA1 samples were nearly identical, with SK_{obs} values of -0.47 and -0.45, respectively, for the first binding event and SK_{obs} values of -0.53 and -0.51 for the second event (Table 3). These results indicate that removal of the IgA1 *N*-glycans causes no detectable alteration in the binding affinity or electrostatic component of binding.

Discussion

Human IgA shares the same basic architecture with other human antibody isotypes, although it has several unusual properties. For example, similar to IgM, IgA is capable of forming higher-order polymeric forms in serum that are formed via interactions between the tailpiece and the J-chain polypeptide. Furthermore, the IgA1 subclass features both *N*- and *O*-glycosylation, with the *O*-glycans restricted to the hinge region whereas the *N*-glycans are present at N263 in the C_H2 domain and N459 in the tailpiece of each heavy chain. The C_H2 *N*-glycans are themselves atypical, in that they are found on the solvent-exposed surface of the Fc region rather than being sequestered between the upper Ig domains of the Fc region, as in IgG and IgE. This exposed nature of the IgA1 *N*-glycans suggests that they may play a role in modulating interactions with IgA-specific receptors such as Fc α RI and Fc α / μ R, or with lectin-like receptors such as mannose-binding lectin and the asialoglycoprotein receptor (45,46). Although the crystal structure of the Fc α RI:Fc α complex yielded a wealth of information about the interface formed between the two proteins, several important questions remained unresolved. In particular, what are the contributions of the C_H2 *N*-glycan and the IgA tailpiece to the IgA1-Fc α RI interface? The structure of the complex showed that the C_H2 *N*-glycan approaches at least within 8 Å of the receptor. However, due to poorly resolved electron density, only one

branch of the complex *N*-glycan was visible. Furthermore, the Fc α fragment crystallized was produced in CHO cells rather than human B cells and thus may not represent the physiological glycoform. Secondly, the Fc α fragment crystallized did not contain the hinge or tailpiece regions. Superimposing our Fc α RI:Fc α complex structure on a model of intact IgA1 determined by small-angle X-ray and neutron scattering suggests that the likely folded-back tailpiece conformations predicted by solution scattering could interfere with or modulate Fc α RI binding (Figure 1B) (9,14). Thus, we have carried out detailed studies of the interaction between Fc α RI and full-length monomeric IgA1 purified from human serum and compared the binding parameters to those for the Fc α :Fc α RI interaction. In humans, circulatory IgA1 is present mainly in its monomeric form with very little polymeric IgA1 (1). However, in diseases such as IgAN, the ratio of polymeric IgA1 to monomeric IgA1 is increased (1,2). Our sedimentation velocity experiments on serum-derived intact myeloma IgA1 proteins κ , λ and Mce showed well-resolved peaks corresponding to IgA1 monomer, dimer/trimer, higher polymer as well as very large-molecular-weight species that could be protein aggregates. This analytical ultracentrifugation approach yields higher-resolution discrimination of the components of serum-derived IgA1 than can be achieved by size exclusion chromatography. Thus, AUC analysis could be useful in studying the polymeric distribution of IgA1 in patients with IgAN or other diseases associated with increased polymeric IgA levels. Interestingly, the mIgA1_{Mce} myeloma protein that exhibits undergalactosylation of the hinge region *O*-glycans (similar to IgAN antibodies) showed a size distribution that was skewed toward larger polymeric species compared to the IgA1 κ and IgA1 λ samples, suggesting a possible link between undergalactosylation of the hinge region and altered polymeric distribution, as previously proposed (47–51).

Our kinetic and equilibrium biosensor studies comparing the binding of Fc α RI to either Fc α or mIgA1 showed small but significant differences in affinity, suggesting that the hinge or tailpiece regions may modulate the interaction. An overlay of the Fc α -Fc α RI crystal structure and the intact IgA1 solution structure suggested that the hinge region is 20–30 Å away from the receptor-binding site (Figure 1A). Therefore, neither the hinge region nor its *O*-glycans are likely to approach Fc α RI in the complex and would at most be expected to contribute only minor long-range electrostatic effects. In contrast, the predicted location of the IgA1 tailpiece clashes with Fc α RI in the modeled complex (Figure 1B). We therefore carried out detailed analyses of the pH- and NaCl-dependence of binding in order to compare the chemical nature of the binding interfaces when Fc α or mIgA1 bind Fc α RI. The binding affinity was reduced as the pH was lowered from 7.0 to 5.5, consistent with protonation of a single histidine residue between neutral and acidic pH, as previously reported for Fc α (11). The NaCl dependence of binding showed a similar slope for both Fc α and mIgA1 binding to Fc α RI, indicating that less than 15% of the free energy of binding was contributed by electrostatics. Thus, the number and nature of ionizable groups in the interface as well as the electrostatic component of binding are similar in the presence or absence of the tailpiece, which contains a histidine, two acidic residues, and potential sialylated *N*-glycans. This suggests that the tailpiece may not play an important role in the IgA1:Fc α RI interface, although these results could depend on the experimental setup used for SPR.

We analyzed the *N*-glycan population on mIgA1 κ and mIgA1 λ samples by use of high-resolution FT-ICR mass spectrometry. Our work expands on prior studies analyzing IgA1 *N*-glycosylation (16,52–54), given that our comprehensive analyses of *N*-glycopeptides and released *N*-glycans allows discrimination of individual glycoforms present within a particular IgA1 sample at each glycosylation site. The high mass accuracy and resolution of FT-ICR MS allows the unambiguous assignment of individual glycoforms. This is especially true in the analysis of *N*-glycosylation where the varied combination of sugars and base peptides can result in a series of *N*-glycan assignments with mass differences less than one atomic mass unit. MS/MS analysis by collision-induced dissociation and IRMPD confirmed the *N*-glycan structure.

In some cases, individual *N*-glycans were observed attached to two or three unique tryptic IgA1 fragments due to unexpected trypsin cleavage sites and variably modified C471 and M461. Taken together, the complete analysis of *N*-glycans as *N*-glycopeptides and PNGase F-released *N*-glycans both with and without neuraminidase treatment provided us with a high level of confidence in the assigned glycans at the two IgA1 sites (Table 5). Furthermore, the combined analyses give us high confidence that we completely characterized the tailpiece *N*-glycans for mIgA1 κ and mIgA1 λ and have identified those *N*-glycans that are unique to the C_H2 site. We observed that many of the *N*-glycan structures were found in both samples, although their relative abundances were distinctly different and there were individual glycoforms that differed between samples, such as tetraantennary *N*-glycans being observed only in the tailpiece of mIgA1 λ . Additionally, mostly biantennary *N*-glycans were observed at the C_H2 site in mIgA1 κ , whereas mostly triantennary *N*-glycans were assigned to the C_H2 in mIgA1 λ . In fact, a greater abundance of triantennary *N*-glycans was observed at both sites in mIgA1 λ .

A comparison of our results with previous analyses of IgA *N*-glycosylation (4,52–54) shows generally similar conclusions, in that the most commonly observed *N*-glycans were complex biantennary and triantennary (or bisecting biantennary) *N*-glycans showing high levels of sialylation and fucosylation. Baenziger and Kornfeld identified three complex *N*-glycans from a myeloma IgA1 sample; all were sialylated biantennary complex *N*-glycans, one of which had a bisecting GlcNAc and another glycan with core fucosylation (52). We observed all the glycans reported by Baenziger, except that we found a monosialylated variant of their disialylated species (IIB). Endo and colleagues analyzed several myeloma IgA1 and IgA2 samples and reported a high degree of variability in the *N*-glycan species between samples (4), similar to our findings here. The majority of the glycans reported by Endo *et al.* are biantennary complex *N*-glycans, about half of which contain bisecting GlcNAc and half of which are fucosylated. They also reported low levels of degalactosylated (i.e., Gal₀) complex *N*-glycans and high-mannose *N*-glycans, neither of which we observed. Field *et al.* analyzed serum-derived (not myeloma-derived) IgA and reported primarily biantennary complex *N*-glycans with variable levels of sialylation and fucosylation, as well as a few triantennary glycans (54). Like Endo *et al.*, they also found low levels of degalactosylated and high-mannose *N*-glycans. Finally, Mattu *et al.* analyzed serum-derived and recombinant IgA and reported a range of biantennary and triantennary species with variable sialylation and fucosylation (53). We observed all the glycans they reported in their serum-derived IgA sample (although our approach cannot resolve the sialic acid linkages or core *vs.* outer-arm fucose attachment). They also observed low levels of degalactosylated and high-mannose *N*-glycans, but only in their recombinant IgA sample. Our data differs from the previous studies in that we observed tetraantennary *N*-glycans (or possibly triantennary glycans with bisecting GlcNAc) in the mIgA1 λ sample that had not previously been reported from serum-derived IgA samples, although Mattu *et al.* did report a single tetraantennary species from recombinant IgA (53). Our results also reveal the degree of variability between individual *N*-glycosylation sites; in particular, only 1 of 8 observed C_H2 glycans for both mIgA1 κ and mIgA1 λ were fucosylated, compared to 19 of 21 tailpiece glycans. These results suggest that differences in accessibility of the *N*-glycans attached to the C_H2 and tailpiece sites likely modulate the activity of the fucosyltransferases involved.

Despite the observed variation in *N*-glycans between mIgA1 samples, kinetic and equilibrium SPR analyses revealed that mIgA1 κ , mIgA1 λ , and mIgA1_{Mce} bound Fc α RI with very similar kinetic parameters and with nearly identical affinities (Figure 3, Tables 1 and 2). Moreover, binding studies with different salt concentrations indicated that all three IgA1 monomers showed similar behavior on binding to Fc α RI (Table 3), indicating that variation in the C_H2 *N*-glycans did not affect Fc α RI affinity. Indeed, even after near-complete enzymatic removal of the IgA1 *N*-glycans, the binding curves for deglycosylated and control mIgA1 κ superimposed precisely, with essentially identical kinetic rate constants, equilibrium

dissociation constants, and salt dependence parameters (Figure 7, Tables 1, 2, and 3). Taken together, these results establish that despite physical proximity, the C_{H2} N-glycans of IgA1 do not play a significant role in the interaction with FcαRI.

Contradictory results have been published regarding the importance of IgA1 C_{H2} N-glycans in binding to FcαRI. Other groups have shown that removal of the IgA1 C_{H2} N-glycan by mutagenesis or enzymatic deglycosylation results in either: i) no effect on FcαRI binding (53), ii) a moderate increase in initial binding (55), or iii) complete loss of binding to FcαRI (56). Many previous binding analyses have tended toward either quantitative biophysical binding analyses using recombinant IgA1 or IgA1-Fc (11,57) or qualitative binding experiments using intact human IgA1 (53,55,56). We have used three different intact IgA1 proteins with native glycosylation purified from human serum in careful quantitative SPR analyses in an attempt to resolve the controversy.

A second ongoing question relates to the role that the IgA tailpiece plays in FcαRI binding. Our kinetic and equilibrium SPR results are in agreement with the studies suggesting that neither the tailpiece peptide nor the N-glycans play a significant role in FcαRI binding (53, 56,58). In these studies, IgA1 mutants, including N263A that lacks the C_{H2} N-glycan and a tailpiece mutant lacking the tailpiece and its N-glycan, were able to bind neutrophil FcαRI and mediate rosette formation to the same extent as wild type IgA1. However, our results are in contrast to qualitative SPR results from Oortwijn *et al.* (55), who reported that removal of the N-glycans from serum IgA resulted in apparent enhanced association and rapid dissociation of mIgA1 with FcαRI by SPR. The two SPR studies were set up differently, however; Oortwijn *et al.* coupled an Fc-FcαRI fusion to the SPR chip and injected IgA1, whereas we coupled IgA1 to the chip and injected soluble FcαRI. Coupling FcαRI to the chip mimics the physiological setting, although we prefer coupling IgA1 in order to improve precision of K_D determinations (11). Finally, our results differ from those of Carayannopoulos *et al.*, who reported that an IgA1 mutant (N263Q using our numbering scheme) lacking the C_{H2} N-glycan expressed in insect cells did not interact with neutrophil FcαRI (56). This discrepancy might be due to a specific effect of the glutamine residue introduced or the expression of IgA1 in insect cells rather than mammalian cells.

Our results are particularly relevant to studies of pathogenesis of IgA nephropathy, as IgAN patients have been widely reported to show aberrant glycosylation of IgA1, along with higher prevalence of polymeric IgA1 forms in serum. Moreover, soluble FcαRI has been implicated in the pathogenesis of IgAN using an FcαRI-transgenic mouse model of IgAN (33). IgA1 glycan abnormalities reported in IgAN patients include oversialylation (27,51), undersialylation (29), and galactose deficiency of hinge-region O-glycans (20,21,25,26,29, 51,59,60), as well as oversialylation (24) or truncation (28) of the N-glycans. Our results indicate that N-glycan truncation is not responsible for modulating the interaction with FcαRI. It is, however, possible that altered IgA1 polymerization may play a role in modulating the functional interaction with FcαRI, and that aberrantly glycosylated IgA1 could play an indirect role as well. Undergalactosylation and undersialylation of IgA1 O-glycans have been reported to cause the IgA1 to aggregate or form immune complexes (21,25,47–50), which is consistent with our sedimentation analysis of IgA1_{Mcc}. Higher-order IgA1 polymeric forms would be expected to show increased avidity of binding to cell-surface FcαRI and would likely be more effective at activating inflammatory pathways and inducing shedding of FcαRI. Future studies will be needed to carefully compare the intrinsic affinity of monomeric and polymeric forms of IgA1 for FcαRI, as well as their functional properties.

Supplementary Material

Refer to Web version on PubMed Central for supplementary material.

Acknowledgements

We thank George Ibrahim for making the Fc α construct, Dr. Jost Vielmetter and Inderjit Nangiana of the Caltech Protein Expression Center for expression of Fc α RI, Mrs. Rhubell Brown for technical assistance, and Dr. Sohaib Khan for use of the Biacore 3000 instrument.

Abbreviations

IgA1	Immunoglobulin alpha 1
Fc	crystallizable fragment
GlcNAc	N-acetyl glucosamine
ADCC	antibody-dependent cell-mediated cytotoxicity
D1	domain 1
AUC	analytical ultracentrifugation
SPR	surface plasmon resonance
IgG	Immunoglobulin gamma
IgE	Immunoglobulin epsilon
IgAN	IgA nephropathy
FT-ICR MS	Fourier transform ion cyclotron resonance mass spectrometry
DMEM	Dulbecco's Modified Eagle's Medium
FBS	fetal bovine serum
TBS	Tris-buffered saline
SDS-PAGE	sodium dodecylsulfate-polyacrylamide gel electrophoresis
PBS	phosphate-buffered saline
RU	response units

MES	morpholino-ethane sulfonic acid
LTQ	two-dimensional linear quadrupole ion trap
IRMPD	infra-red multiphoton dissociation

References

1. Monteiro RC, Van De Winkel JG. IgA Fc receptors. *Annu Rev Immunol* 2003;21:177–204. [PubMed: 12524384]
2. Mestecky, J.; Moro, I.; Kerr, MA.; Woof, JM. *Mucosal Immunology*. Mestecky, J.; Bienenstock, J.; Lamm, ME.; Mayer, L.; McGhee, JR.; Strober, W., editors. 3. Elsevier Academic Press; Amsterdam: 2005. p. 153-181.
3. Putnam FW, Liu YS, Low TL. Primary structure of a human IgA1 immunoglobulin. IV Streptococcal IgA1 protease, digestion, Fab and Fc fragments, and the complete amino acid sequence of the α 1 heavy chain. *J Biol Chem* 1979;254:2865–2874. [PubMed: 107164]
4. Endo T, Mestecky J, Kulhavy R, Kobata A. Carbohydrate heterogeneity of human myeloma proteins of the IgA1 and IgA2 subclasses. *Mol Immunol* 1994;31:1415–1422. [PubMed: 7823967]
5. Maliszewski CR, March CJ, Schoenborn MA, Gimpel S, Shen L. Expression cloning of a human Fc receptor for IgA. *J Exp Med* 1990;172:1665–1672. [PubMed: 2258698]
6. Monteiro RC, Kubagawa H, Cooper MD. Cellular distribution, regulation, and biochemical nature of an Fc α receptor in humans. *J Exp Med* 1990;171:597–613. [PubMed: 2137852]
7. van Zandbergen G, Westerhuis R, Mohamad NK, van De Winkel JG, Daha MR, van Kooten C. Crosslinking of the human Fc receptor for IgA (Fc α RI/CD89) triggers FcR gamma-chain-dependent shedding of soluble CD89. *J Immunol* 1999;163:5806–5812. [PubMed: 10570263]
8. van der Boog PJ, van Zandbergen G, de Fijter JW, Klar-Mohamad N, van Seggelen A, Brandtzaeg P, Daha MR, van Kooten C. Fc α RI/CD89 circulates in human serum covalently linked to IgA in a polymeric state. *J Immunol* 2002;168:1252–1258. [PubMed: 11801662]
9. Herr AB, Ballister ER, Bjorkman PJ. Insights into IgA-mediated immune responses from the crystal structures of human Fc α RI and its complex with IgA1-Fc. *Nature* 2003;423:614–620. [PubMed: 12768205]
10. Woof JM, Burton DR. Human antibody-Fc receptor interactions illuminated by crystal structures. *Nat Rev Immunol* 2004;4:89–99. [PubMed: 15040582]
11. Herr AB, White CL, Milburn C, Wu C, Bjorkman PJ. Bivalent Binding of IgA1 to Fc α RI Suggests a Mechanism for Cytokine Activation of IgA Phagocytosis. *J Mol Biol* 2003;327:645–657. [PubMed: 12634059]
12. Garman SC, Wurzburg BA, Tarchevskaya SS, Kinet JP, Jardetzky TS. Structure of the Fc fragment of human IgE bound to its high-affinity receptor Fc ϵ RI α . *Nature* 2000;406:259–266. [PubMed: 10917520]
13. Sondermann P, Huber R, Oosthuizen V, Jacob U. The 3.2-Å crystal structure of the human IgG1 Fc fragment-Fc γ RIII complex. *Nature* 2000;406:267–273. [PubMed: 10917521]
14. Boehm MK, Woof JM, Kerr MA, Perkins SJ. The Fab and Fc fragments of IgA1 exhibit a different arrangement from that in IgG: a study by X-ray and neutron solution scattering and homology modelling. *J Mol Biol* 1999;286:1421–1447. [PubMed: 10064707]
15. Rifai A, Fadden K, Morrison SL, Chintalacheruvu KR. The N-glycans determine the differential blood clearance and hepatic uptake of human immunoglobulin (Ig)A1 and IgA2 isotypes. *J Exp Med* 2000;191:2171–2182. [PubMed: 10859341]
16. Royle L, Roos A, Harvey DJ, Wormald MR, van Gijlswijk-Janssen D, Redwan el RM, Wilson IA, Daha MR, Dwek RA, Rudd PM. Secretory IgA N- and O-glycans provide a link between the innate and adaptive immune systems. *J Biol Chem* 2003;278:20140–20153. [PubMed: 12637583]

17. Basset C, Durand V, Jamin C, Clement J, Pennec Y, Youinou P, Dueymes M, Roitt IM. Increased N-linked glycosylation leading to oversialylation of monomeric immunoglobulin A1 from patients with Sjögren's syndrome. *Scand J Immunol* 2000;51:300–306. [PubMed: 10736100]
18. Saulsbury FT. Alterations in the O-linked glycosylation of IgA1 in children with Henoch-Schönlein purpura. *J Rheumatol* 1997;24:2246–2249. [PubMed: 9375892]
19. Lau KK, Wyatt RJ, Moldoveanu Z, Tomana M, Julian BA, Hogg RJ, Lee JY, Huang WQ, Mestecky J, Novak J. Serum levels of galactose-deficient IgA in children with IgA nephropathy and Henoch-Schönlein purpura. *Pediatr Nephrol* 2007;22:2067–2072. [PubMed: 17943324]
20. Moldoveanu Z, Wyatt RJ, Lee JY, Tomana M, Julian BA, Mestecky J, Huang WQ, Anreddy SR, Hall S, Hastings MC, Lau KK, Cook WJ, Novak J. Patients with IgA nephropathy have increased serum galactose-deficient IgA1 levels. *Kidney Int* 2007;71:1148–1154. [PubMed: 17342176]
21. Tomana M, Novak J, Julian BA, Matousovich K, Konecny K, Mestecky J. Circulating immune complexes in IgA nephropathy consist of IgA1 with galactose-deficient hinge region and antiglycan antibodies. *J Clin Invest* 1999;104:73–81. [PubMed: 10393701]
22. Monteiro RC, Moura IC, Launay P, Tsuge T, Haddad E, Benhamou M, Cooper MD, Arcos-Fajardo M. Pathogenic significance of IgA receptor interactions in IgA nephropathy. *Trends Mol Med* 2002;8:464–468. [PubMed: 12383768]
23. Emancipator, SN. *Heptinstall's Pathology of the Kidney*. Jennette, JC.; Olson, JL.; Schwartz, MM.; Silva, FG., editors. Lippincott-Raven Publishers; Philadelphia: 1998. p. 479-539.
24. Linossier MT, Palle S, Berthoux F. Different glycosylation profile of serum IgA1 in IgA nephropathy according to the glomerular basement membrane thickness: normal versus thin. *Am J Kidney Dis* 2003;41:558–564. [PubMed: 12612978]
25. Mestecky J, Tomana M, Crowley-Nowick PA, Moldoveanu Z, Julian BA, Jackson S. Defective galactosylation and clearance of IgA1 molecules as a possible etiopathogenic factor in IgA nephropathy. *Contrib Nephrol* 1993;104:172–182. [PubMed: 8325028]
26. Hiki Y, Odani H, Takahashi M, Yasuda Y, Nishimoto A, Iwase H, Shinzato T, Kobayashi Y, Maeda K. Mass spectrometry proves under-O-glycosylation of glomerular IgA1 in IgA nephropathy. *Kidney Int* 2001;59:1077–1085. [PubMed: 11231363]
27. Leung JC, Tang SC, Chan DT, Lui SL, Lai KN. Increased sialylation of polymeric lambda-IgA1 in patients with IgA nephropathy. *J Clin Lab Anal* 2002;16:11–19. [PubMed: 11835525]
28. Amore A, Cirina P, Conti G, Brusa P, Peruzzi L, Coppo R. Glycosylation of circulating IgA in patients with IgA nephropathy modulates proliferation and apoptosis of mesangial cells. *J Am Soc Nephrol* 2001;12:1862–1871. [PubMed: 11518779]
29. Odani H, Hiki Y, Takahashi M, Nishimoto A, Yasuda Y, Iwase H, Shinzato T, Maeda K. Direct evidence for decreased sialylation and galactosylation of human serum IgA1 Fc O-glycosylated hinge peptides in IgA nephropathy by mass spectrometry. *Biochem Biophys Res Commun* 2000;271:268–274. [PubMed: 10777713]
30. Grossetete B, Launay P, Lehuen A, Jungers P, Bach JF, Monteiro RC. Down-regulation of Fcα receptors on blood cells of IgA nephropathy patients: evidence for a negative regulatory role of serum IgA. *Kidney Int* 1998;53:1321–1335. [PubMed: 9573548]
31. van Zandbergen G, van Kooten C, Mohamad NK, Reterink TJ, de Fijter JW, van de Winkel JG, Daha MR. Reduced binding of immunoglobulin A (IgA) from patients with primary IgA nephropathy to the myeloid IgA Fc-receptor, CD89. *Nephrol Dial Transplant* 1998;13:3058–3064. [PubMed: 9870466]
32. Moura IC, Arcos-Fajardo M, Sadaka C, Leroy V, Benhamou M, Novak J, Vrtovnik F, Haddad E, Chintalacharuvu KR, Monteiro RC. Glycosylation and size of IgA1 are essential for interaction with mesangial transferrin receptor in IgA nephropathy. *J Am Soc Nephrol* 2004;15:622–634. [PubMed: 14978164]
33. Launay P, Grossetete B, Arcos-Fajardo M, Gaudin E, Torres SP, Beaudoin L, Patey-Mariaud de Serre N, Lehuen A, Monteiro RC. Fcα receptor (CD89) mediates the development of immunoglobulin A (IgA) nephropathy (Berger's disease). Evidence for pathogenic soluble receptor-IgA complexes in patients and CD89 transgenic mice. *J Exp Med* 2000;191:1999–2009. [PubMed: 10839814]
34. Moura IC, Centelles MN, Arcos-Fajardo M, Malheiros DM, Collawn JF, Cooper MD, Monteiro RC. Identification of the transferrin receptor as a novel immunoglobulin (Ig)A1 receptor and its enhanced

- expression on mesangial cells in IgA nephropathy. *J Exp Med* 2001;194:417–425. [PubMed: 11514599]
35. van der Boog PJ, De Fijter JW, Van Kooten C, Van Der Holst R, Van Seggelen A, Van Es LA, Daha MR. Complexes of IgA with Fc α RI/CD89 are not specific for primary IgA nephropathy. *Kidney Int* 2003;63:514–521. [PubMed: 12631116]
 36. van der Boog PJ, van Kooten C, van Zandbergen G, Klar-Mohamad N, Oortwijn B, Bos NA, van Remoortere A, Hokke CH, de Fijter JW, Daha MR. Injection of recombinant Fc α RI/CD89 in mice does not induce mesangial IgA deposition. *Nephrol Dial Transplant* 2004;19:2729–2736. [PubMed: 15340093]
 37. Renfrow MB, Mackay CL, Chalmers MJ, Julian BA, Mestecky J, Kilian M, Poulsen K, Emmett MR, Marshall AG, Novak J. Analysis of O-glycan heterogeneity in IgA1 myeloma proteins by Fourier transform ion cyclotron resonance mass spectrometry: implications for IgA nephropathy. *Anal Bioanal Chem* 2007;389:1397–1407. [PubMed: 17712550]
 38. Tomana M, Prchal JT, Garner LC, Skalka HW, Barker SA. Gas chromatographic analysis of lens monosaccharides. *J Lab Clin Med* 1984;103:137–142. [PubMed: 6690636]
 39. Renfrow MB, Cooper HJ, Tomana M, Kulhavy R, Hiki Y, Toma K, Emmett MR, Mestecky J, Marshall AG, Novak J. Determination of aberrant O-glycosylation in the IgA1 hinge region by electron capture dissociation fourier transform-ion cyclotron resonance mass spectrometry. *J Biol Chem* 2005;280:19136–19145. [PubMed: 15728186]
 40. Schuck P. Size-distribution analysis of macromolecules by sedimentation velocity ultracentrifugation and lamm equation modeling. *Biophys J* 2000;78:1606–1619. [PubMed: 10692345]
 41. Myszka DG, Morton TA. CLAMP: a biosensor kinetic data analysis program. *TIBS* 1998;23:149–150. [PubMed: 9584619]
 42. Record MT Jr, Lohman ML, De Haseth P. Ion effects on ligand-nucleic acid interactions. *J Mol Biol* 1976;107:145–158. [PubMed: 1003464]
 43. Bradshaw JM, Waksman G. Calorimetric investigation of proton linkage by monitoring both the enthalpy and association constant of binding: application to the interaction of the Src SH2 domain with a high-affinity tyrosyl phosphopeptide. *Biochemistry* 1998;37:15400–15407. [PubMed: 9799501]
 44. Tanaka A, Iwase H, Hiki Y, Kokubo T, Ishii-Karakasa I, Toma K, Kobayashi Y, Hotta K. Evidence for a site-specific fucosylation of N-linked oligosaccharide of immunoglobulin A1 from normal human serum. *Glycoconj J* 1998;15:995–1000. [PubMed: 10211705]
 45. Gomes MM, Herr AB. IgA and IgA-specific receptors in human disease: structural and functional insights into pathogenesis and therapeutic potential. *Springer Semin Immunopathol* 2006;28:383–395. [PubMed: 17043868]
 46. Hamburger AE, Bjorkman PJ, Herr AB. Structural insights into antibody-mediated mucosal immunity. *Curr Top Microbiol Immunol* 2006;308:173–204. [PubMed: 16922091]
 47. Iwase H, Ohkawa S, Ishii-Karakasa I, Hiki Y, Kokubo T, Sano T, Tanaka A, Toma K, Kobayashi Y, Hotta K. Study of the relationship between sticky human serum IgA1 and its O-glycan glycoform. *Biochem Biophys Res Commun* 1999;261:472–477. [PubMed: 10425209]
 48. Iwase H, Tanaka A, Hiki Y, Kokubo T, Sano T, Ishii-Karakasa I, Toma K, Kobayashi Y, Hotta K. Aggregated human serum immunoglobulin A1 induced by neuraminidase treatment had a lower number of O-linked sugar chains on the hinge portion. *J Chromatogr B Biomed Sci Appl* 1999;724:1–7. [PubMed: 10202952]
 49. Kokubo T, Hiki Y, Iwase H, Tanaka A, Toma K, Hotta K, Kobayashi Y. Protective role of IgA1 glycans against IgA1 self-aggregation and adhesion to extracellular matrix proteins. *J Am Soc Nephrol* 1998;9:2048–2054. [PubMed: 9808090]
 50. Kokubo T, Hiki Y, Iwase H, Horii A, Tanaka A, Nishikido J, Hotta K, Kobayashi Y. Evidence for involvement of IgA1 hinge glycopeptide in the IgA1-IgA1 interaction in IgA nephropathy. *J Am Soc Nephrol* 1997;8:915–919. [PubMed: 9189858]
 51. Suzuki H, Moldoveanu Z, Hall S, Brown R, Vu HL, Novak L, Julian BA, Tomana M, Wyatt RJ, Edberg JC, Alarcon GS, Kimberly RP, Tomino Y, Mestecky J, Novak J. IgA1-secreting cell lines from patients with IgA nephropathy produce aberrantly glycosylated IgA1. *J Clin Invest* 2008;118:629–639. [PubMed: 18172551]

52. Baenziger J, Kornfeld S. Structure of the carbohydrate units of IgA1 immunoglobulin. I Composition, glycopeptide isolation, and structure of the asparagine-linked oligosaccharide units. *J Biol Chem* 1974;249:7260–7269. [PubMed: 4436308]
53. Mattu TS, Pleass RJ, Willis AC, Kilian M, Wormald MR, Lellouch AC, Rudd PM, Woof JM, Dwek RA. The glycosylation and structure of human serum IgA1, Fab, and Fc regions and the role of N-glycosylation on Fc α receptor interactions. *J Biol Chem* 1998;273:2260–2272. [PubMed: 9442070]
54. Field MC, Amatayakul-Chantler S, Rademacher TW, Rudd PM, Dwek RA. Structural analysis of the N-glycans from human immunoglobulin A1: comparison of normal human serum immunoglobulin A1 with that isolated from patients with rheumatoid arthritis. *Biochem J* 1994;299(Pt 1):261–275. [PubMed: 8166649]
55. Oortwijn BD, Roos A, van der Boog PJ, Klar-Mohamad N, van Remoortere A, Deelder AM, Daha MR, van Kooten C. Monomeric and polymeric IgA show a similar association with the myeloid Fc α RI/CD89. *Mol Immunol* 2007;44:966–973. [PubMed: 16675016]
56. Carayannopoulos L, Max EE, Capra JD. Recombinant human IgA expressed in insect cells. *Proc Natl Acad Sci U S A* 1994;91:8348–8352. [PubMed: 8078886]
57. Wines BD, Hulett MD, Jamieson GP, Trist HM, Spratt JM, Hogarth PM. Identification of residues in the first domain of human Fc α receptor essential for interaction with IgA. *J Immunol* 1999;162:2146–2153. [PubMed: 9973489]
58. Pleass RJ, Dunlop JI, Anderson CM, Woof JM. Identification of residues in the CH2/CH3 domain interface of IgA essential for interaction with the human Fc α receptor (Fc α R) CD89. *J Biol Chem* 1999;274:23508–23514. [PubMed: 10438530]
59. Lai KN, Chan LY, Tang SC, Tsang AW, Guo H, Tse KC, Yip T, Leung JC. Characteristics of polymeric lambda-IgA binding to leukocytes in IgA nephropathy. *J Am Soc Nephrol* 2002;13:2309–2319. [PubMed: 12191975]
60. Moore JS, Kulhavy R, Tomana M, Moldoveanu Z, Suzuki H, Brown R, Hall S, Kilian M, Poulsen K, Mestecky J, Julian BA, Novak J. Reactivities of N-acetylgalactosamine-specific lectins with human IgA1 proteins. *Mol Immunol* 2007;44:2598–2604. [PubMed: 17275907]

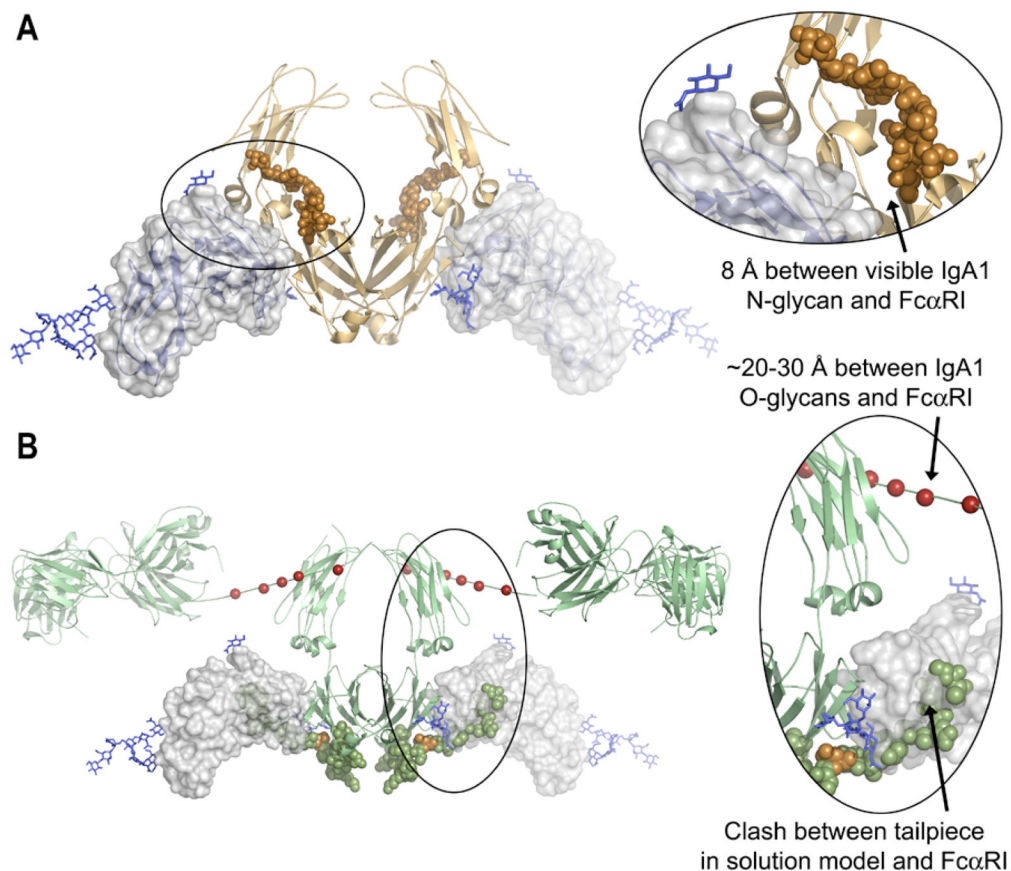


Figure 1. Structural views of the IgA1 N-glycans and tailpiece

(A) Crystal structure of the FcαRI:Fcα complex (pdb 1OW0, reference (9)), showing that the C_H2 N-glycan on IgA1 (copper spheres) approaches FcαRI (blue ribbons and transparent surface) but does not directly contact the receptor. The electron density for the N-glycan was weak and only one branch of the complex carbohydrate was visible.

(B) Docking of FcαRI from the FcαRI:Fcα complex onto the low-resolution solution scattering structure of intact IgA1 (pdb 1IGA, reference (14)). The deposited IgA1 model illustrates one possible location for the IgA1 tailpiece, which is shown as green spheres, with N459 (the location of the tailpiece N-glycan) in gold. Note that in this potential orientation the tailpiece clashes with FcαRI, and that the potential hinge O-glycosylation sites (red spheres) are distant from FcαRI.

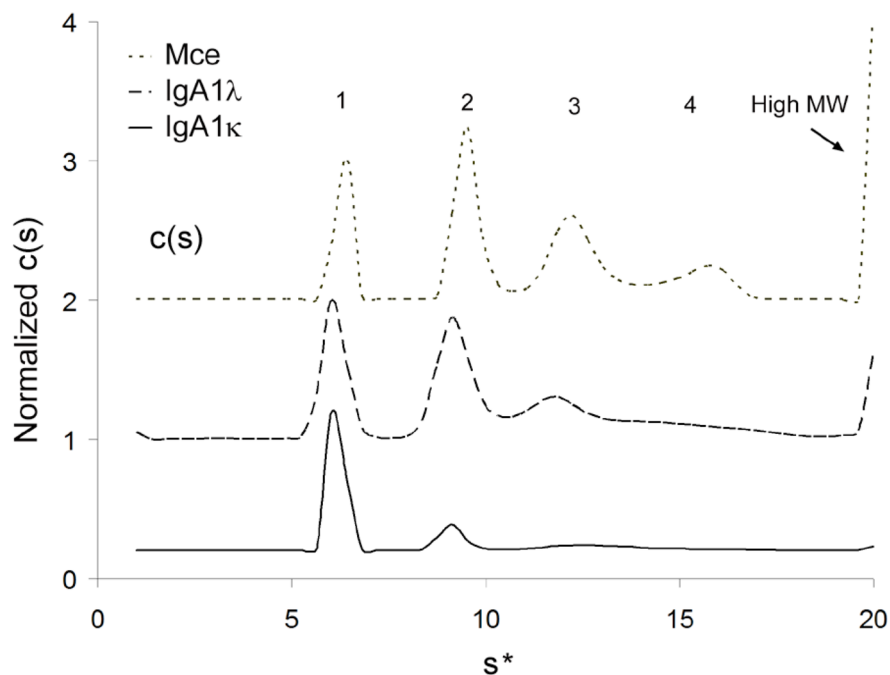


Figure 2. Sedimentation Velocity Analysis of IgA1 κ , λ and Mce

IgA1 κ , λ and Mce samples were spun at 36,000 rpm in a Beckman XL-I analytical ultracentrifuge. Data were fitted using the $c(s)$ and $c(M)$ sedimentation analysis routines in the program SEDFIT, which yielded the differential distribution coefficients of the sedimenting species for each sample. Distinct peaks corresponding to monomeric (labeled “1”), dimeric (“2”), trimeric (“3”) and polymeric (“4”) IgA1 species could be resolved from high molecular weight aggregates in all three samples analyzed.

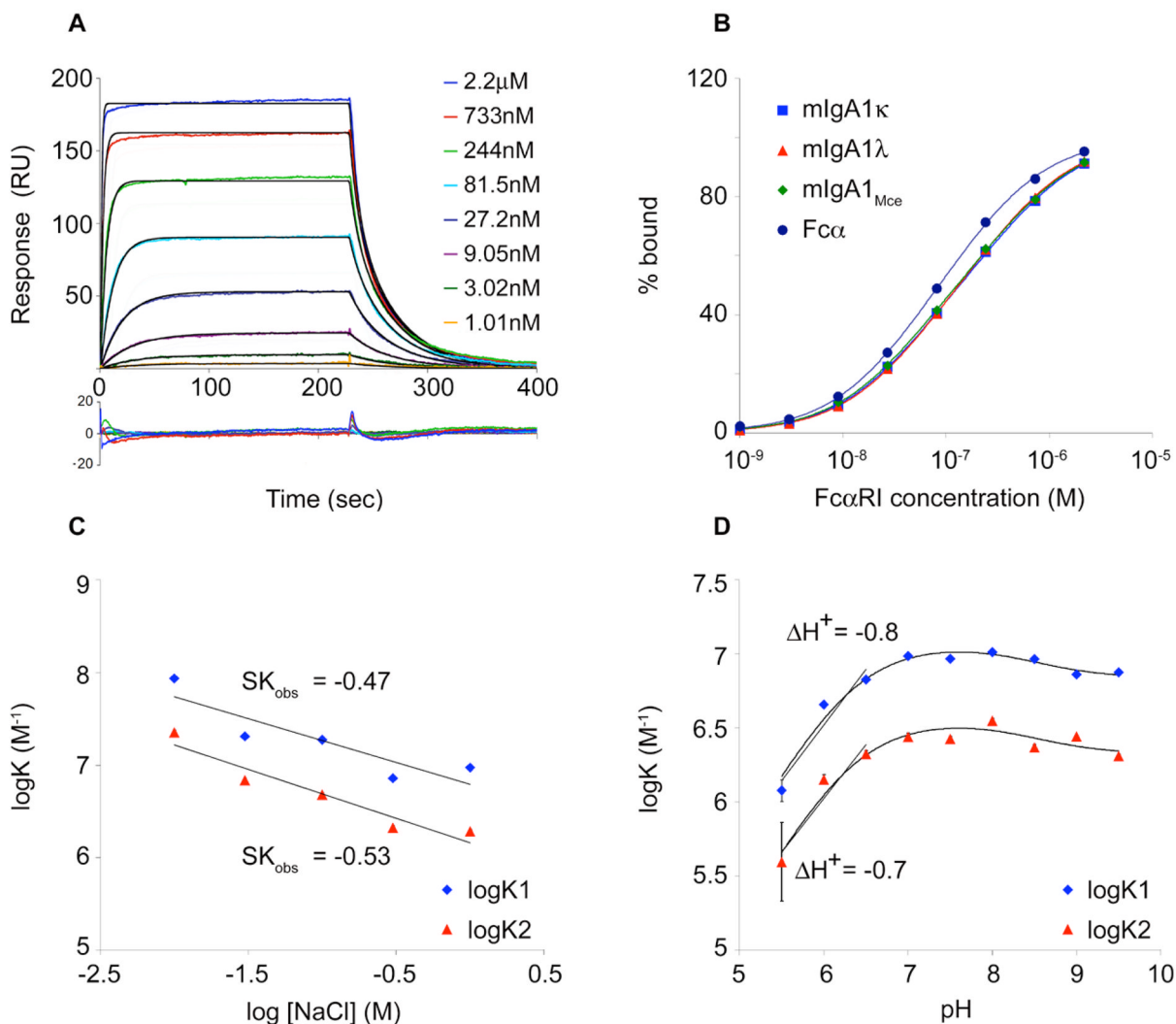


Figure 3. Surface plasmon resonance analysis of the Fc α RI:mIgA1 or Fc α interaction

(A) Representative sensograms derived from injection of different concentrations of Fc α RI over mIgA1 κ . Kinetic data were fit globally using the bivalent ligand model (black lines) in the program ClampXP. A residual plot is shown beneath the data. (B) Equilibrium binding isotherms for Fc α RI binding to Fc α and mIgA1 κ , λ and Mce. Data points were determined by averaging the equilibrium response at the plateau of each kinetic curve and fitted to a two-site model (solid lines) in the program Scientist. (C) Analysis of salt dependence of mIgA1 κ binding to Fc α RI. Association equilibrium constants K1 (blue diamonds) and K2 (red triangles) for each of the two binding events were determined as a function of [NaCl] from kinetic parameters. The slope of this plot (SK_{obs}) was determined for each binding event by linear regression. (D) Analysis of pH dependence of mIgA1 κ binding to Fc α RI. Binding constants K1 (blue diamonds) and K2 (red triangles) for each binding event were determined as a function of pH from kinetic parameters. Data were fitted to a model of linked protonation and binding equilibria in the program Scientist. In addition, the slope of each curve yields ΔH^+ , the net number of protons released or taken up on binding. ΔH^+ of -0.8 and -0.7 for the first and second binding event, respectively, suggest, a single ionizable residue is present at each Fc α RI:mIgA1 binding interface.

and Y₂). Additional fragments from the terminal end (B₃, B₄) further confirm the *N*-glycan structure. Symbols for the individual monosaccharide residues are defined in the key. Distinction between Gal and Man monosaccharides is assumed based on our monosaccharide compositional analysis and previously reported IgA1 *N*-glycan analysis (4,52–54). Some individual *N*-glycan fragments are assigned to two possible bonds due to their isobaric composition. B) IRMPD FT-ICR MS/MS spectrum of the same IgA1 *N*-glycan shown in panel A, analyzed as a PNGase F-released glycan. In addition to the pattern of *N*-glycan fragments similar to those in A, monosaccharide losses which can only be attributed to the reducing end are observed (highlighted in red). The NeuAc residue is arbitrarily assigned to the β branch to simplify the labeled spectra.

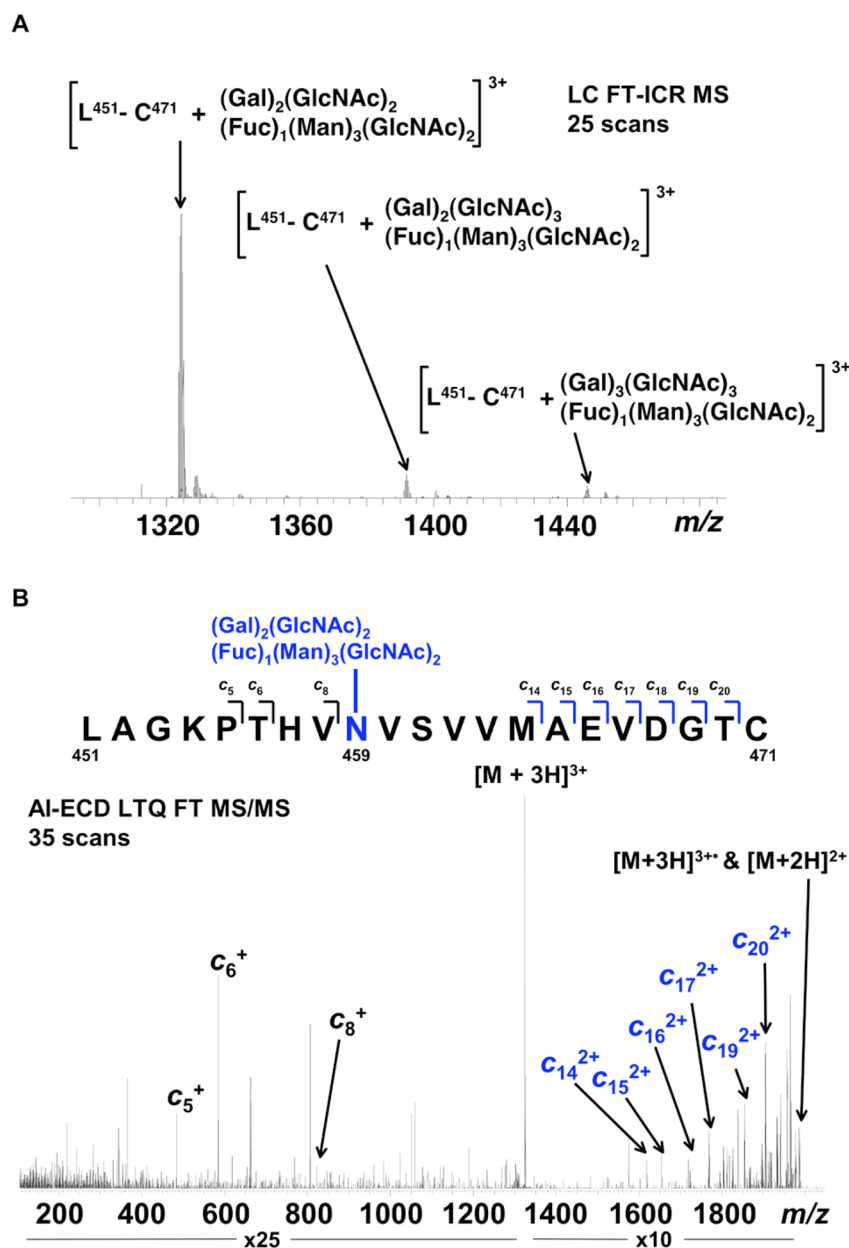


Figure 5. Representative FT-ICR data for mIgA1κ N-glycans

(A) FT-ICR MS spectrum from the average of 25 LC FT-ICR MS scans revealing the presence of three distinct mIgA1κ N-glycopeptides. Each N-glycopeptide corresponds to the mass of the IgA1 peptide L451-C471 with three related but distinct glycans. (B) AI-ECD FT-ICR tandem mass spectrum of the $[\text{L}^{451}\text{-C}^{471} + (\text{Gal})_2(\text{GlcNAc})_2(\text{Fuc})_1(\text{Man})_3(\text{GlcNAc})_2]^{3+}$ triply charged ion species confirms the peptide sequence as the tailpiece (N459) site of mIgA1κ. A total of ten c type fragments were observed, originating from the N-terminus. Seven fragments C-terminal to N459 correspond to the mass of the IgA1 tryptic peptide plus the mass of the attached glycan, in contrast to the three fragments N-terminal to N459. The mass accuracy of the three IgA1 tailpiece N-glycans shown in (A) are as follows: L451-C471 + $(\text{Gal})_2(\text{GlcNAc})_2(\text{Fuc})_1(\text{Man})_3(\text{GlcNAc})_2$ —theoretical mass 3968.714, measured mass 3968.724, error 2.52 ppm; L451-C471 + $(\text{Gal})_2(\text{GlcNAc})_3(\text{Fuc})_1(\text{Man})_3(\text{GlcNAc})_2$ —

theoretical mass 4171.793, measured mass 4171.806, error 3.24 ppm; L451-C471 + (Gal)₃(GlcNAc)₃(Fuc)₁(Man)₃(GlcNAc)₂—theoretical mass 4333.846, measured mass 4333.848, error 0.67 ppm. Table 5 lists the identified IgA1 *N*-glycans identified for both mIgA1κ and mIgA1λ.

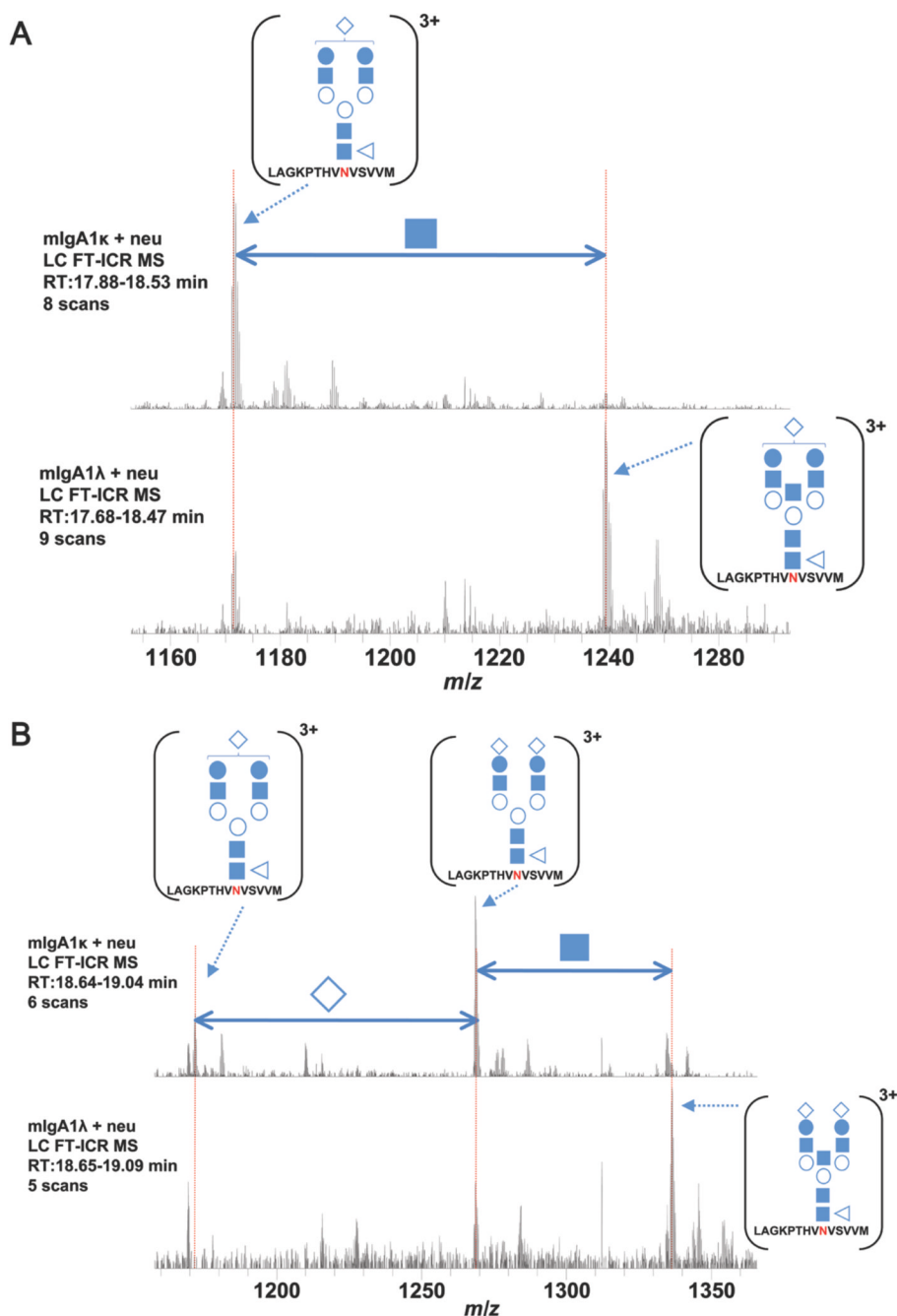


Figure 6. The distribution of *N*-glycans differs between mIgA1κ and mIgA1λ.

Extracted FT-ICR MS spectra from two independent LC MS analyses of mIgA1κ and mIgA1λ. The two LC MS runs are compared at different points in the chromatogram. At the first aligned retention time (A) the spectra reveal a mono-sialylated IgA1 tryptic peptide [L451-M464]³⁺ that is observed predominantly as a biantennary *N*-glycopeptide in mIgA1κ (biantennary vs. triantennary abundance > 10:1). In contrast, the same two IgA1 *N*-glycopeptides observed in mIgA1λ have a different relative abundance (biantennary vs. triantennary abundance ~1:3), with the triantennary *N*-glycoform dominating. This same pattern holds later in the analysis of a disialylated version of the same IgA1 tryptic peptide (B) Similar relative abundances were observed for each sample in the released *N*-glycan analysis

(data not shown). The position of the bisecting biantennary IgA1 *N*-glycan is assumed based on previous work (4,53). Monosaccharide nomenclature is the same as in Figure 4.

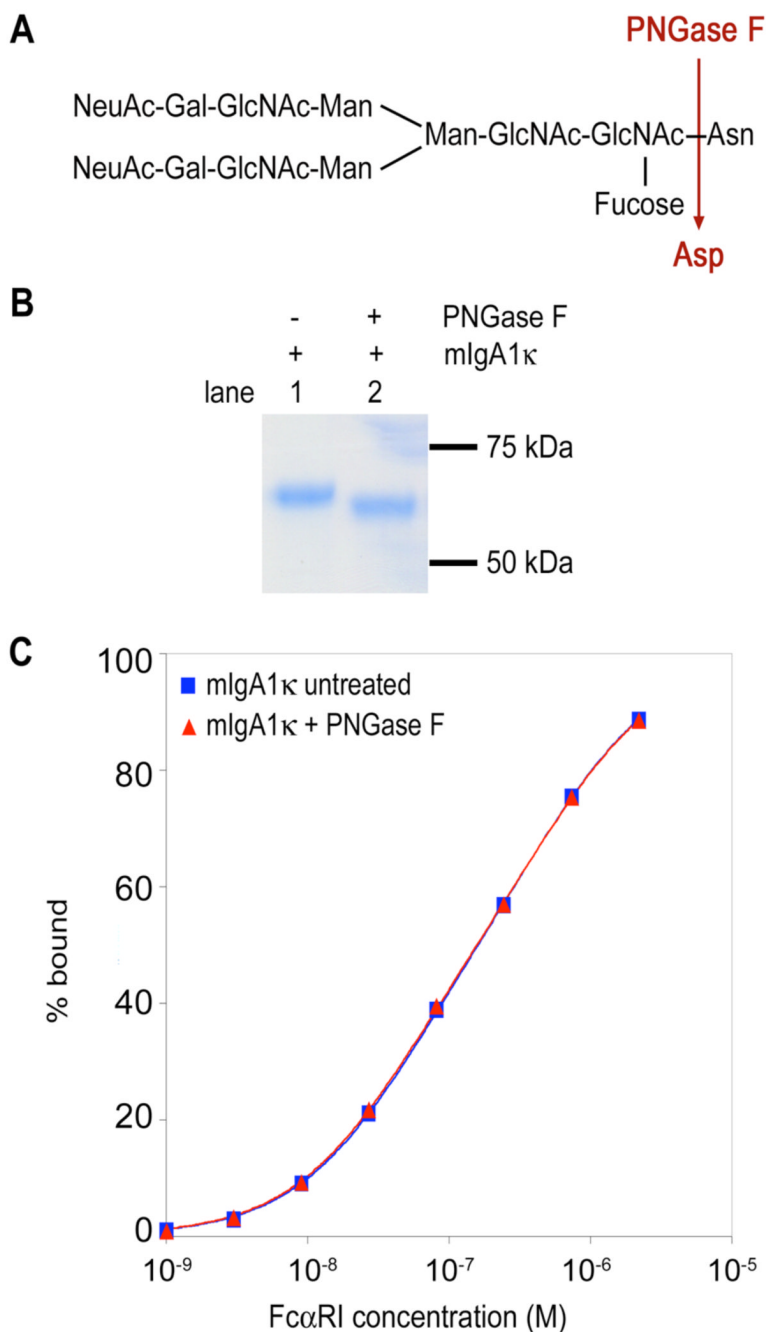


Figure 7. Enzymatic deglycosylation of mIgA1 κ N-glycans

(A) Structure of a typical biantennary complex N-glycan and the site of enzymatic deglycosylation. (B) Reducing SDS-PAGE gel stained with Coomassie blue to show the shift in migration of heavy chain after deglycosylation. (C) Equilibrium binding isotherm for Fc α RI binding to mIgA1 κ before and after enzymatic deglycosylation. Data points were determined by averaging the equilibrium response at the plateau of each kinetic curve and fitted to a two-site model (solid lines) in the program Scientist. Fc α RI bound similarly to both native and deglycosylated mIgA1 κ samples.

TABLE 1
Kinetic parameters for Fc α RI interactions with Fc α , mIgA1 κ , λ , and Mce at 25° C
 Kinetic rate constants were determined using the bivalent ligand model in the program ClampXP.

Ligand	Analyte	$k_{1on} (M s)^{-1a}$	$k_{1off} (s^{-1})$	$k_{2on} (M s)^{-1}$	$k_{2off} (s^{-1})^a$	$K_{p1} (nM)$	$K_{p2} (nM)$
Fc α	Fc α RI	4.61×10^5	0.0278	4.47×10^5	0.054	60.4 ± 0.3	121 ± 1
mIgA1 κ ^b	Fc α RI	3.55×10^5	0.0266	3.04×10^5	0.074	74.9 ± 0.4	244 ± 4
mIgA1 λ	Fc α RI	3.12×10^5	0.0254	5.25×10^5	0.102	81.5 ± 0.7	195 ± 6
mIgA1 _{Mce}	Fc α RI	3.65×10^5	0.0264	4.56×10^5	0.101	72.3 ± 0.8	222 ± 8
mIgA1 κ ^c	Fc α RI	3.17×10^5	0.0267	3.15×10^5	0.096	84.1 ± 0.6	303 ± 8
Deglycosylated mIgA1 κ ^c	Fc α RI	3.29×10^5	0.0258	1.87×10^5	0.060	78.4 ± 0.6	320 ± 7

^aRate constants k_{1on} and k_{2off} have been corrected by statistical factors, as described in Experimental Procedures.

^bKinetic parameters for mIgA1 κ listed here were derived from a global analysis of three independent experiments, each with eight different concentrations of injected analyte.

^cKinetic parameters for mIgA1 κ before and after deglycosylation were determined from a single batch of mIgA1 κ in order to more precisely determine the specific effects of glycosylation.

TABLE 2**Equilibrium parameters for Fc α RI binding to Fc α , mIgA1 κ , λ and Mce**

K_D values were determined using a two-site model in the program Scientist.

	K_{D1} (nM)	K_{D2} (nM)
Fc α	36.1 \pm 1.6	204 \pm 15
mIgA1 κ ^a	40.2 \pm 1.9	452 \pm 58
mIgA1 λ	47.6 \pm 1.2	371 \pm 21
mIgA1 _{Mce}	40.8 \pm 1.7	403 \pm 40
mIgA1 κ	45.0 \pm 0.9	571 \pm 37
Deglycosylated mIgA1 κ	42.6 \pm 1.0	582 \pm 45

^aEquilibrium constants for mIgA1 κ were derived from global analysis of three independent experiments each with eight different concentrations of injected analyte.

TABLE 3**NaCl dependence of Fc α and mIgA1 κ , λ and Mce binding to Fc α RI**

Slopes (SK_{obs}) for each binding event were determined by fitting $\log K_A$ (derived from kinetic rate constants) to a linear regression model. The electrostatic component of the Gibbs free energy of binding ($\Delta G_{elec}/\Delta G$) was determined by comparing the ΔG at 10mM with that at 1M NaCl. ΔG was determined using the formula $\Delta G = -RT \ln K_A$ where K_A is the association constant, R is the gas constant in cal ($K^{-1} \text{ mol}^{-1}$), and T is the temperature in Kelvin.

	High affinity site		Low affinity site	
	SK_{obs}	$\Delta G_{elec}/\Delta G$	SK_{obs}	$\Delta G_{elec}/\Delta G$
Fc α	-0.32	8.2%	-0.36	9.3%
mIgA1 κ	-0.47	12%	-0.53	15%
Deglycosylated mIgA1 κ	-0.45	11%	-0.51	14%
mIgA1 λ	-0.51	12%	-0.51	14%
mIgA1 $_{Mce}$	-0.60	15%	-0.42	11%

TABLE 4

Linked binding/protonation equilibrium analysis of Fc α and mIgA1k binding to Fc α RI

Parameters were determined using a linked binding/protonation model with two ionizable residues per binding site in the program Scientist, as described in Experimental Procedures.

Ligand	High affinity site K_b (nM)	Low affinity site K_b (nM)	(pK $_a$) $_f$	(pK $_a$) $_b$	(pK $_a$) $_f$	(pK $_a$) $_b$
Fc α	79.9 \pm 1.95	187 \pm 45.7	6.5 \pm 0.25	~4.0	8.1 \pm 0.93	8.4 \pm 0.92
mIgA1k	88.0 \pm 1.15	287 \pm 37.6	6.3 \pm 0.17	~4.0	8.4 \pm 0.60	8.6 \pm 0.61

TABLE 5
FT-ICR Mass spectrometry analysis of N-glycans on mIgA1κ and mIgA1λ.

Glycopeptides from tryptic digests were analyzed to determine site-specific N-glycoforms. In parallel, N-glycans released by PNGase F treatment were analyzed for comparison. Both sets of samples were tested with and without neuraminidase treatment. The summary lists the assigned location(s) of each observed glycoform: either N263 (CH2) or N459 in the tailpiece (TP).

	mIgA1κ			mIgA1λ		
	✓	✓	Summary	✓	✓	Summary
Trypsin:						
PNGase F:						
Neuraminidase:						
Glycoforms						
Biantennary						
(Gal) ₂ (GlcNAc) ₂ + (Man) ₃ (GlcNAc) ₂	□	◆	◆	□	◆	◆
(NeuAc) ₁ (Gal) ₁ (GlcNAc) ₂ + (Man) ₃ (GlcNAc) ₂	◆	◆	◆	◆	◆	◆
(NeuAc) ₁ (Gal) ₂ (GlcNAc) ₂ + (Man) ₃ (GlcNAc) ₂	◆	◆	◆	◆	◆	◆
(NeuAc) ₂ (Gal) ₂ (GlcNAc) ₂ + (Man) ₃ (GlcNAc) ₂	◆	◆	◆	◆	◆	◆
(Gal) ₂ (GlcNAc) ₂ + (Fuc) ₁ (Man) ₃ (GlcNAc) ₂	□	◆	◆	□	◆	◆
(NeuAc) ₁ (Gal) ₂ (GlcNAc) ₂ + (Fuc) ₁ (Man) ₃ (GlcNAc) ₂	□	◆	◆	□	◆	◆
(NeuAc) ₂ (Gal) ₂ (GlcNAc) ₂ + (Fuc) ₁ (Man) ₃ (GlcNAc) ₂	□	◆	◆	□	◆	◆
Triantennary						
(Gal) ₁ (GlcNAc) ₃ + (Man) ₃ (GlcNAc) ₂						
(Gal) ₂ (GlcNAc) ₃ + (Man) ₃ (GlcNAc) ₂						
(NeuAc) ₁ (Gal) ₂ (GlcNAc) ₃ + (Man) ₃ (GlcNAc) ₂						
(Gal) ₂ (GlcNAc) ₃ + (Fuc) ₁ (Man) ₃ (GlcNAc) ₂						
(NeuAc) ₁ (Gal) ₂ (GlcNAc) ₃ + (Fuc) ₁ (Man) ₃ (GlcNAc) ₂						
(NeuAc) ₂ (Gal) ₂ (GlcNAc) ₃ + (Fuc) ₁ (Man) ₃ (GlcNAc) ₂						
(Gal) ₃ (GlcNAc) ₃ + (Fuc) ₁ (Man) ₃ (GlcNAc) ₂						
(NeuAc) ₁ (Gal) ₃ (GlcNAc) ₃ + (Fuc) ₁ (Man) ₃ (GlcNAc) ₂						
(NeuAc) ₂ (Gal) ₃ (GlcNAc) ₃ + (Fuc) ₁ (Man) ₃ (GlcNAc) ₂						
(NeuAc) ₃ (Gal) ₃ (GlcNAc) ₃ + (Fuc) ₁ (Man) ₃ (GlcNAc) ₂						
Tetraantennary						
(Gal) ₃ (GlcNAc) ₄ + (Fuc) ₁ (Man) ₃ (GlcNAc) ₂						
(NeuAc) ₂ (Gal) ₃ (GlcNAc) ₄ + (Fuc) ₁ (Man) ₃ (GlcNAc) ₂						
(NeuAc) ₃ (Gal) ₃ (GlcNAc) ₄ + (Fuc) ₁ (Man) ₃ (GlcNAc) ₂						

□ denotes verified tailpiece N-glycans from tryptic glycopeptide analysis

◆ denotes verified CH2 N-glycans from tryptic glycopeptide analysis

◆ denotes N-glycans released by PNGase F treatment

◆ denotes the assignment of the N-glycans to the CH2 or tailpiece sites.

For simplicity, all glycans containing (Gal)₂(GlcNAc)₃ are listed as triantennary rather than bisecting biantennary; likewise, all glycans containing (Gal)₃(GlcNAc)₄ are listed as tetraantennary.